Solar Energy 220 (2021) 578–589

Contents lists available at ScienceDirect

Solar Energy

journal homepage: www.elsevier.com/locate/solener

Energy partitioning and spatial variability of air temperature, VPD and radiation in a greenhouse tunnel shaded by semitransparent organic PV modules

Maayan Friman-Peretz [a,b], Shay Ozer [a], Asher Levi [a], Esther Magadley [c], Ibrahim Yehia [c], Farhad Geoola [a], Shelly Gantz [d], Roman Brikman [a], Avi Levy [b], Murat Kacira [e], Meir Teitel [a,*]

[a] Institute of Agricultural Engineering, Agricultural Research Organization, The Volcani Center, HaMaccabim Road 68, P.O. Box 15159, Rishon LeZion 7528809, Israel
[b] Department of Mechanical Engineering, Ben-Gurion University of the Negev, P.O. Box 653, Beer-Sheva 81405, Israel
[c] Triangle Research and Development Center, P.O. Box 2167, Kfar-Qari 30075, Israel
[d] Agricultural Extension Service of Israel – Shaham, Ministry of Agriculture, HaMaccabim Road 68, Rishon LeZion, P. O. Box 30, Beit Dagan 50200, Israel
[e] Biosystems Engineering, University of Arizona, Tucson, AZ 85721, USA

ARTICLE INFO

Keywords:
Organic photovoltaics
Semitransparent
Solar greenhouse
Microclimate parameters

ABSTRACT

A study related to the application of organic photovoltaic (OPV) modules in greenhouses is presented. It considers the impact of nonhomogeneous shading by semitransparent OPV modules, placed on the cover of a greenhouse tunnel housing a tomato crop, on energy partitioning and the spatial variability of radiation, air temperature and vapour pressure deficit (VPD) within the tunnel. Experiments were conducted in two similar tunnels covered by a diffuse polyethylene sheet. Flexible semitransparent strips of OPV modules were placed on 37% of the roof area of one tunnel, creating an approximately 23% nonhomogeneous shading, while the other tunnel, homogeneously shaded by a 25% black shading net, served as a control greenhouse. The results show that on cloudy days (high diffuse radiation), spatial variability of radiation in the OPV tunnel was smaller than on sunny days (low diffuse radiation). Conversely, variability in air temperature and VPD did not change much with the change in diffuse radiation. Except when diffuse radiation was high, no significant difference in the energy partitioning between nonhomogeneous shading by OPVs and homogeneous shading was observed. Most of the net radiation in the tunnels was converted into latent heat. With a high solar elevation angle, the spatial variability of radiation within the tunnel was higher than with a low solar elevation angle. Additional experiments are needed to determine the best arrangement of semitransparent OPV modules on the roof, without resulting in any significant increase in spatial variability. Agronomic aspects of plant growth under the OPV modules are briefly presented.

1. Introduction

In the last decade, the use of photovoltaics (PVs), both in agricultural open fields or protected cultivation, has increased with increasing desire for renewable energy for a more sustainable world and the need to efficiently use the land. Yano and Cossu (2019) indicated that although the application of PV panels in greenhouses can reduce fuel and grid electricity consumption, PVs inherently conflict with cultivation because both photosynthesis and PVs depend on sunlight availability. The authors further argued that light in greenhouses varies greatly according to whether the PV modules are concentrated as a single array or spread over the roof, and suggested that semitransparent PV panels be used as an effective method for providing more homogeneous shadowing. Their review showed that a chequerboard pattern allowed for a better distribution of solar radiation than a straight-line pattern, wherein direct sunlight was available to the crop often during the day because of the intermittent shading. The authors further emphasised the importance of finding the best methods of applying opaque or semitransparent PV panels on greenhouse roofs in order to minimise crop damage due to shading.

Cossu et al. (2020) argued that the heterogeneity of light distribution inside PV greenhouses should be carefully considered for crop management, especially in terms of transplantation among plant rows, fertigation, and crop protection.

The feasibility of changing the degree of shading inside a greenhouse

* Corresponding author.
E-mail address: grteitel@agri.gov.il (M. Teitel).

https://doi.org/10.1016/j.solener.2021.03.050
Received 5 November 2020; Received in revised form 5 February 2021; Accepted 17 March 2021
Available online 12 April 2021

Nomenclature

C	factor of the non-closure of the energy balance
C_p	specific heat of dry air, J kg^{-1} °C^{-1}
G	soil heat flux, W m^{-2}
h	heat transfer coefficient, W °C^{-1} m^{-2}
l	characteristic leaf length, m
m_w	ratio between the molecular weights of water vapour and dry air
P_{atm}	atmospheric pressure, kPa
r_a	aerodynamic resistance, s m^{-1}
r_c	stomatal resistance, s m^{-1}
Re	Reynolds number
R_G	global radiation, W m^{-2}
R_{G0}	ambient global radiation, W m^{-2}
$R.H.$	relative humidity of tunnel air, %
R.H.$_0$	ambient relative humidity, %
R_n	net radiation, W m^{-2}
S	sensible heat flux, W m^{-2}
T_a	air temperature, °C, or K
T_{leaf}	average canopy temperature, °C
T_0	ambient air temperature, °C
u	air velocity, m s^{-1}
U_0	ambient wind speed, m s^{-1}
V_{pair}	air vapor pressure, kPa
V_{psat}	saturation pressure, kPa
VPD	water vapour pressure deficit, kPa

Greek letters

γ	psychrometric constant, kPa °C^{-1}
η	Power conversion efficiency, %
Δ	slope of the saturation vapour pressure curve, kPa °C^{-1}
λ	latent heat of vaporisation, J kg^{-1}
λE	latent heat flux, W m^{-2}
ρ	air density, kg m^{-3}

Abbreviations

LAI	Leaf area index
OPV	Organic photovoltaic
PAR	Photosynthetically active radiation
PV	Photovoltaic
PPFD	Photosynthetic photon flux density

based on the available solar radiation and plant needs was tested and reported by Moretti and Marucci (2019). Thus, the change in shading degree was obtained via panel rotation.

Chen et al. (2019) proposed a numerical method to predict the radiation distribution and electricity production of a PV greenhouse over the year by utilising a 3D model that considered both shortwave and thermal radiation. Simulations of three PV greenhouse configurations in straight-line, crisscross, and chequerboard PV panel layouts were conducted. The performance of each configuration was evaluated in terms of the non-uniformity of the radiation distribution, radiation intensity, and electricity production. The non-uniformity of the hourly radiation under the straight-line layout was not very different from that of the crisscross and chequerboard layouts. However, compared with the straight line and crisscross layouts, the annual electricity production of the chequerboard layout was higher.

Cossu et al. (2017a) introduced a novel algorithm to estimate the cumulated global radiation inside PV greenhouses in order to select the most suitable plant species according to its light needs. The solar radiation distribution was calculated using direct and diffuse radiation, wherein the authors assessed the periods when the shadow projected by the PV array cast covered specific observation points within the greenhouse. Most zones close to the sidewalls and gable walls were the least affected by shading at all canopy heights.

Using a computational fluid dynamic (CFD) model, Fatnassi, Poncet, Bazzano, Brun, and Bertin (2015) determined the solar radiation distribution, air temperature, water vapour, and other parameters in two different greenhouse prototypes (asymmetric and Venlo) that had PV panels on their roof. Two arrangements of PV panel array were tested: straight-line and chequerboard. The data analysis revealed that (i) solar radiation is more evenly distributed in the Venlo greenhouse than in the asymmetric greenhouse; (ii) Compared with the straight-line arrangement, the chequerboard PV panel setup improved the spatial distribution of sunlight transmitted into the greenhouse.

Also using CFD simulations, Baxevanou et al. (2020) assessed the effect of placing semitransparent organic PVs (OPVs) on the polyethylene cover of a greenhouse roof on the available photosynthetically active radiation (PAR) inside the greenhouse. Three coverage ratios that gave transmittances of 30%, 45%, and 60% were examined. PAR isocontours showed that the PAR distribution changed during the day and that these changes varied among the different coverage ratios considered.

Marucci, Monarca, Colantoni, Campiglia, and Cappuccini (2017) analysed the shading variation inside a tunnel greenhouse outfitted with flexible transparent PV panels in a checkerboard arrangement. The variation and distribution of the shading percentage of the PV panels were analysed in relation to the coverage percentage of the roof area, the total area of the greenhouse, and the different sections of the greenhouse. From mid-March to mid-September, shading during the middle of the day was always inside the greenhouse. Meanwhile, during other months, shading occurred partly inside and partly outside the tunnel greenhouse.

The light distribution in a PV greenhouse with an entire roof area covered with PV panels was calculated by Cossu et al. (2017b). The calculation of the incident global radiation was estimated under clear sky conditions for several observation points located inside the greenhouse. The results were shown through a map of light distribution over the greenhouse area, which highlighted the most penalised zones and the percentage of available global radiation as compared with the same greenhouse without a PV array. The zones close to the gable walls and south side wall suffered less shading as compared with the central region.

Tani, Shiina, Nakashima, and Hayashi (2014) discovered the possibility of improving lettuce growth by using light diffusion films under roof-mounted PV modules. Their results suggested that the application of light diffusion films is a viable option for improving crop productivity under roof-mounted PV modules as diffused light penetrates the lower layers of the canopy, thereby increasing the CO_2 fixation of the whole canopy.

Thus, it is evident that shading by PV panels placed on the top of a greenhouse cover is one of the most crucial problems regarding PV greenhouses. Therefore, integrating PV panels in greenhouse farms has raised concerns regarding the sustainability of this specific agrosystem in terms of crop planning and management (Cossu et al., 2020). In particular, the desire to generate a homogeneous shade distribution continues to be a major challenge. Partial coverage of greenhouse roofs, the use of semitransparent PV modules, and the use of PVs combined with diffuse films as a greenhouse cover have been proposed to improve the solar radiation distribution within greenhouses. Specifically, semitransparent panels appear to be a suitable solution for use in PV greenhouses. Among the semitransparent materials, dye-sensitised solar cells (DSSCs) or OPVs appear to have great potential for use in protected cultivation.

Over the last decade, several studies have been performed to examine the application of OPV technology in greenhouses (Magadley et al., 2020; Friman-Peretz et al., 2019, 2020; Zhang et al., 2018; Okada et al., 2018; dos Reis Benatto et al., 2017; Emmott et al., 2015, 2016; Yang et al., 2015). These studies investigated different aspects, including electricity produced under various OPV coverage ratios and angles, mean daily power conversion efficiency, stability issues, degradation, and the spectral selectivity of the modules.

Despite increasing interest and research regarding the application of OPV technology in greenhouses, the effect on the spatially distributed microclimate and the spatial variability within the plants, as well as the resulting dynamic nonhomogeneous shading, due to the partial coverage of greenhouse roofs with semitransparent OPV modules, has not been comprehensively investigated. This study mostly builds on the data collected during experiments described in Friman-Peretz et al. (2020). It examines the spatial variability in radiation, air temperature and VPD in a greenhouse high tunnel equipped with OPV strips on the roof. Then, a comparison is performed between energy partitioning in homogeneous and nonhomogeneous shaded tunnels, under sunny and cloudy days, to determine the effect of shading type and percentage of diffuse radiation in the global solar radiation, on the energy partitioning.

2. Materials and methods

2.1. Experimental facility

The experiment was conducted from May to August 2019. For a complete experimental setup, refer to Friman-Peretz et al. (2020). Note, however, that changes to this experimental procedure and methodological modifications were conducted as follows.

On 21 August 2019, the photosynthetic photon flux density (PPFD) was measured using a quantum sensor (LI-COR, Lincoln, NE, USA) along

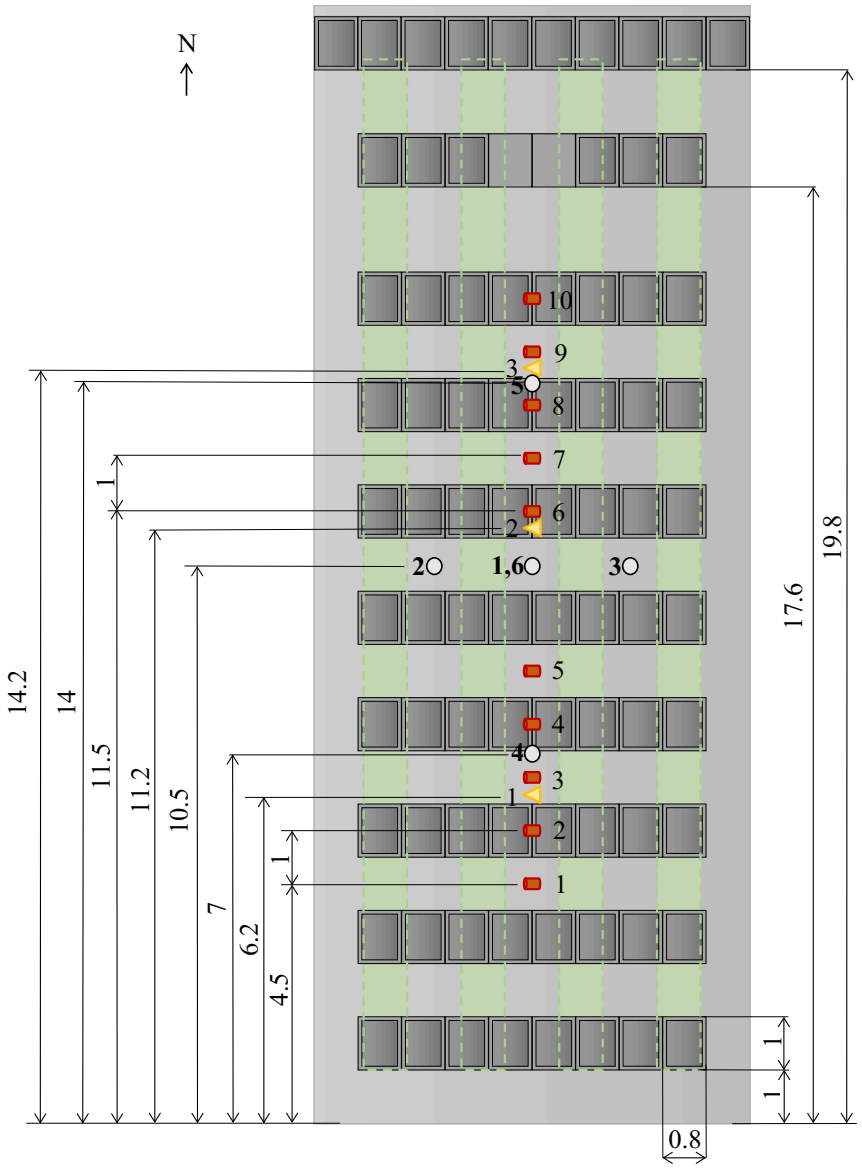

Fig. 1a. Arrangement of organic photovoltaic (OPV) modules (grey horizontal strips) on the top of the OPV greenhouse tunnel as well as the net radiation sensors (◁), global radiation sensors (▬), and dry and wet air temperature sensors in aspirated boxes (○). Vertical green strips represent the four plant rows. Dimensions are in metres. (For interpretation of the references to color in this figure legend, the reader is referred to the web version of this article.)

the paths between adjacent plant beds (not including the paths adjacent to the sidewalls so as to prevent side effects). The sensor was moved at a height of approximately 2.3 m from the ground at three different time periods, 10:36–10:44, 11:55–12:04, and 12:48–12:57 in the OPV tunnel, and 10:47–10:57, 12:06–12:12, and 12:59–13:06 in the control tunnel (a tunnel homogeneously shaded by a 25% black shading net). For each path (of the 3 paths in each tunnel), the sensor was moved twice back and forth. In total, it took approximately 6–10 min to complete the measurements in each tunnel, each time data was collected. The PPFD values were recorded at 4 Hz on a CR6 data logger (Campbell Scientific, Logan, UT, USA).

The leaf area index (LAI) and characteristic leaf length were measured in few days along the growing season by the LI-3050C transparent belt conveyor with a scanning head of the LI-3000C (LI-COR,

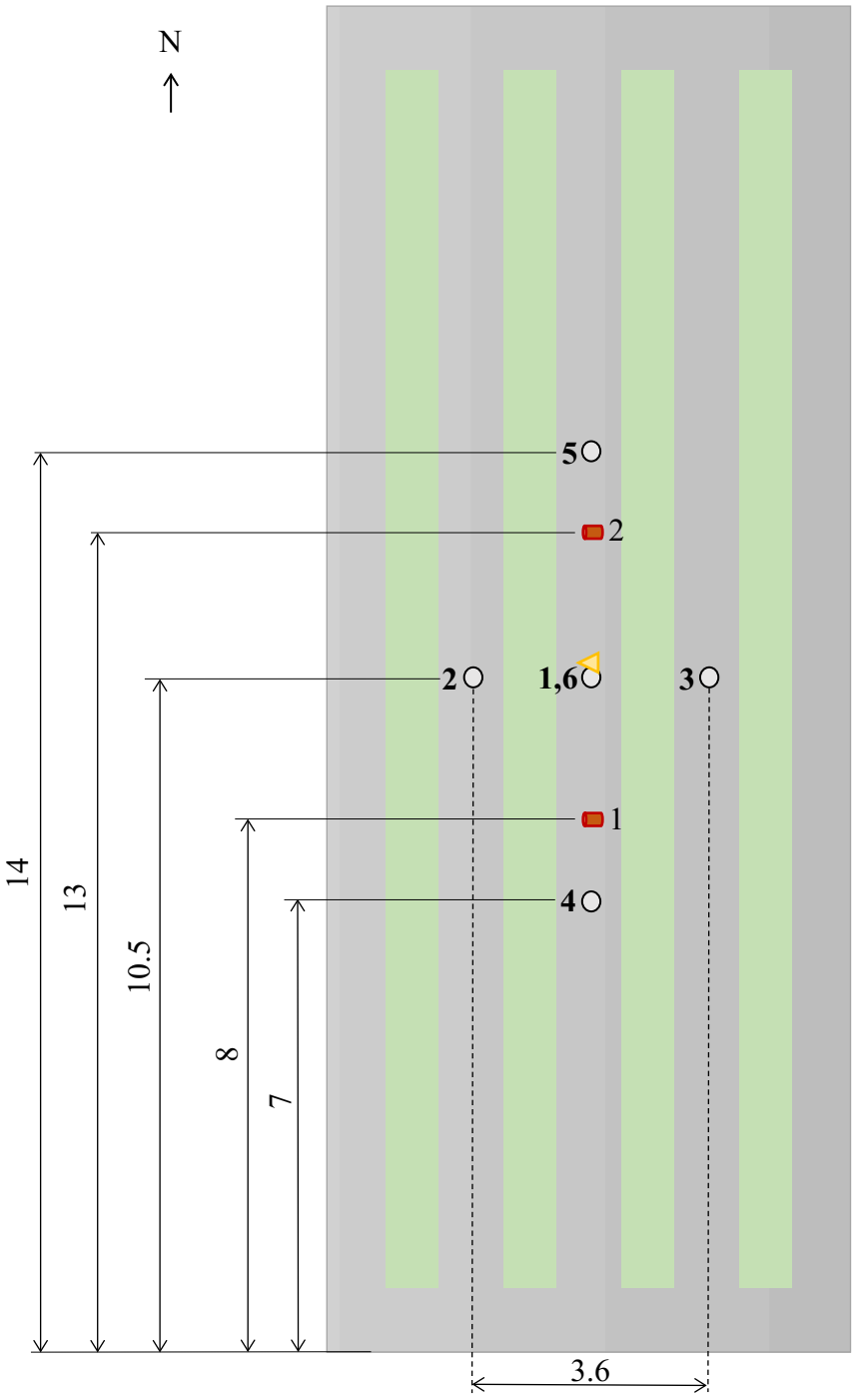

Fig. 1b. Schematic view of sensor positions in the control tunnel. Net radiation sensor (◁), global radiation (▬), dry and wet air temperature in aspirated boxes (○). Vertical green strips represent the four plant rows. Dimensions are in metres. (For interpretation of the references to color in this figure legend, the reader is referred to the web version of this article.)

Table 1
Physical and radiometric properties of the polyetylen cover and OPV modules.

	Polyethylen	OPV module
Thickness mm	0.15	0.6
Density Kg m^{-3}	950	1370
Specific heat J $kg^{-1}K^{-1}$	2100	1275
Thermal conductivity watt m^{-1} K^{-1}	0.33	0.28
Tansmittance 400–700 nm %	82.7	21.4
Reflectance, 400–700 nm %	14.1	14.4
Absroptance, 400–700 nm %	3.2	64.2
Radiation diffusion 400–700 nm %	40	N.A.

Lincoln, NE, USA).

Diffuse radiation was measured using a shadow ring in combination with a SMP3 pyranometer (Kipp & Zonen, Delft, The Netherlands) in addition to all measurements of the external condition described in Friman-Peretz et al. (2020).

Fig. 1a shows a top view of the arrangement of OPV modules on top of the greenhouse tunnel, the net and global radiation sensors position and the position of aspirated boxes to measure air temperature and humidity. Although Fig. 1a was presented in Friman-Peretz et al. (2020) we show it here as well, for the convenience of the reader. Fig. 1b shows a schematic view of sensor positions (net and global radiation sensors and the aspirated boxes) in the control tunnel.

The physical and radiometric properties of the polyethylene film used to cover the tunnel and the OPV modules placed on the cover, are given in Table 1.

The electrical characteristics of the OPV modules are briefly given in the following. For more details, the reader is referred to Friman-Peretz et al. (2019) and Magadley et al. (2020). Under an incident irradiance in the range of 600–1000 Wm^{-2} the open-circuit voltage and short circuit current were in the range of 28–31 V and 0.25–0.39 A. The fill factor changed during the day in the range of 0.24–0.38. The mean daily power conversion efficiency η was equal to about 0.8%, lower than the 2.2% reported by the manufacturer under STC conditions.

2.2. Energy balance and partitioning

The effects of nonhomogeneous shading by the OPV strips and percentage of diffuse radiation in the global solar radiation, on the energy partitioning within the tunnel, was investigated, and a comparison with the energy partitioning in a homogeneously shaded tunnel is discussed herein. Energy partitioning provides information on the fractions of net radiation converted into sensible and latent heat (vapour) fluxes or the sensible and latent heat fluxes exchanged between the canopy and the air within the tunnel at the canopy level. Fig. 2 shows a schematic diagram of the energy fluxes.

The energy balance equation can be written as

$$R_n - G = \lambda E + S \tag{1}$$

where R_n (W m^{-2}) is the net radiation, G (W m^{-2}) is the soil heat flux, λE (W m^{-2}) is the latent heat flux, and S (W m^{-2}) is the sensible heat flux.

The factor C, which characterises the non-closure of the energy balance, can be defined as:

$$C = \frac{\lambda E + S}{R_n - \mathrm{G}} \tag{2}$$

Latent heat flux due to transpiration, λE, is estimated from the canopy-scale version of the Penman-Monteith equation as follows (Monteith and Unsworth, 2013):

$$\lambda E = \frac{\Delta(R_n - \mathrm{G}) + \frac{\rho \cdot C_p \cdot VPD}{r_a}}{\Delta + \gamma\left(1 + \frac{r_c}{r_a}\right)} \tag{3}$$

where Δ (kPa °C^{-1}) is the slope of the saturation vapour pressure curve as a function of average air temperature, ρ (kg m^{-3}) is the air density, C_p (J kg^{-1} °C^{-1}) is the specific heat of the dry air, VPD (kPa) is the water vapour pressure deficit, γ (kPa °C^{-1}) is the psychrometric constant, r_c (s m^{-1}) is the canopy stomatal resistance, and r_a (s m^{-1}) is the canopy aerodynamic resistance.

The VPD is defined as:

$$VPD = V_{psat} - V_{pair}, \tag{4}$$

where the saturation pressure (V_{psat}) is given by (ASHRAE Handbook, 2005):

$$V_{psat}[kPa] = (10^{-3}) \cdot e^{\left(-5.8002206 \cdot \frac{10^3}{T_a[k]}\right) + 1.3914993 - \left(4.8640239 \cdot 10^{-2} \cdot (T_a[k])\right) + \left(4.1764768 \cdot 10^{-5} \cdot (T_a[k])^2\right)} \cdot e^{\left(-1.4452093 \cdot 10^{-8} \cdot (T_a[k])^3\right) + (6.5459673 \cdot Ln(T_a[k]))}, \tag{5}$$

where T_a is the air temperature, and the air vapour pressure (V_{pair}) is:

$$V_{pair}[kPa] = \frac{V_{psat} \cdot R.H.}{100} \tag{6}$$

where $R.H.$(%) is the relative humidity of air inside the tunnel.

The canopy aerodynamic resistance is (Teitel, 2017):

$$r_a = \frac{305}{LAI}\left(\sqrt{\frac{l}{u}}\right), \tag{7}$$

where l (m) is the characteristic length of the leaf (0.113 m in the present study), u (m s^{-1}) is the mean air velocity in the tunnel, and LAI is the leaf area index.

Canopy stomatal resistance can be calculated from the expression given by Villarreal-Guerrero et al. (2012) as follows:

$$r_c = C_1 \cdot \left(\frac{\frac{R_n}{2LAI} + C_2}{\frac{R_n}{2LAI} + C_3}\right) \cdot \left(1 + C_4 \cdot VPD^2\right), \tag{8}$$

where, for a tomato crop, Villarreal-Guerrero et al. (2012) provided the following values: $C_1 = 18.6$, $C_2 = 197.5$, $C_3 = 0.31$, and $C_4 = 1.2 \times 10^{-6}$.

The slope of the saturation vapour pressure curve as a function of temperature, Δ (kPa °C^{-1}), is given by (Tetens, 1930; Murray, 1967):

$$\Delta = \frac{4098\left(0.6108 \cdot exp\left(\frac{17.27T_a}{T_a + 273.3}\right)\right)}{(T_a + 273.3)^2} \tag{9}$$

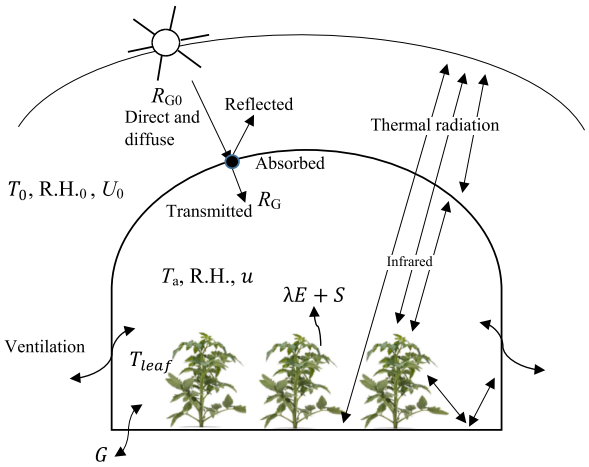

Fig. 2. Schematic diagram of energy partitioning in a greenhouse tunnel.

The psychrometric constant, γ (kPa °C^{-1}) is:

$$\gamma = \frac{C_p \cdot P_{atm}}{\lambda \cdot m_w} = 0.067, \tag{10}$$

where P_{atm} (kPa) is the atmospheric pressure, $\lambda = 2.43 \times 10^{-6}$ (J kg^{-1}) is the latent heat of vaporisation, and $m_w = 0.622$ is the ratio between the molecular weight of water vapour and dry air.

The temperature difference between the leaves and the adjacent air, combined with the airflow due to ventilation results in a thermal boundary layer on the surface of the leaves. Thus, the sensible heat flux between the canopy and air is

$$S = 2h \cdot (T_{leaf} - T_a) \tag{11}$$

where h (W °C^{-1}m^{-2}) is the heat transfer coefficient, and T_{leaf} (°C) is the average canopy temperature.

Finally, the heat transfer coefficient h, which depends on the convection modes and flow types (laminar or turbulent), can be described by:

$$h = \frac{\rho C_p}{r_a}. \tag{12}$$

3. Results and discussion

In a previous paper (Friman-Peretz et al., 2020) it was shown that the nonhomogeneous shading caused by the strips of OPV modules, which covered 37% of the roof (resulting in 23% shading), created almost the same average value of radiation along the tunnel centreline as that observed in the control tunnel that had 25% shading by a black shading net.

In this paper, we concentrate on spatial variability of parameters and first show the effect on the distribution of radiation along the tunnel centreline of nonhomogeneous shading via OPV strips versus homogeneous shading via a net, under different percentages of diffuse solar radiation and different solar elevation angles.

It is noticed that a non-homogenous shading may negatively affect plant growth. To overcome this possible problem, we have used a polyethylene cover film with high light diffusion (40%) so that light is better distributed within the canopy. A further improvement of the light distribution can be obtained by using narrow strips of OPV modules with small spacing between adjacent strips while keeping the desired coverage percentage.

Fig. 3 shows the percentage of diffuse radiation out of the global radiation measured by the meteorological station outside the tunnels. Each point represents the average value of data measured between 11:00 and 13:00 when changes in radiation with time are relatively small and values are expected to be highest on the day. Meanwhile, the circles show the selected dates at the beginning, middle, and toward the end of the experimental period. Three sunny days after the beginning (23–25 June) and toward the end (12–14 August) of the growing season were selected to check the effect of changes in the solar elevation angle on the radiation distribution along the tunnel centreline. Three sunny (14–16 July) and three cloudy days (17, 18, and 21 July) were chosen in the middle of the growing season to examine the effect of the percentage of diffuse radiation on the radiation distribution along the tunnel centrelines.

Fig. 4 examines the influence of nonhomogeneous shading in the OPV tunnel on the radiation distribution along the tunnel centreline. Additionally, it examines the effect of the percentage of ambient diffuse radiation on that distribution. Herein, the radiation values are averages of data measured between 11:00 and 13:00. Note that the radiation values measured by the sensors under shaded areas were significantly lower than those measured by the sensors in the unshaded areas. As expected, the radiation on sunny days was higher than that on cloudy days in the unshaded areas. The difference in radiation values between the shaded and unshaded sensors were higher on sunny days than on cloudy days, wherein there is a high percentage of diffuse radiation.

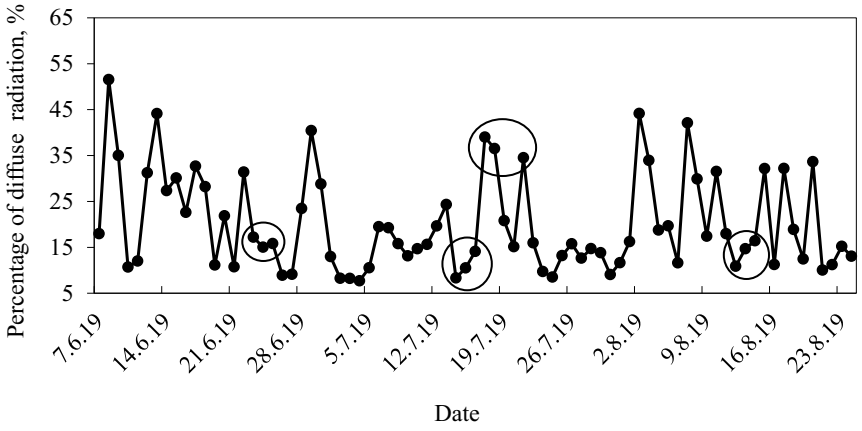

Fig. 3. Percentage of diffuse radiation in ambient radiation between 11:00 and 13:00 during the experimental period. Circles show 3 sunny days with low diffusive radiation after the beginning and toward the end of the growing season, and 6 days (3 sunny and 3 cloudy) in the middle of the season.

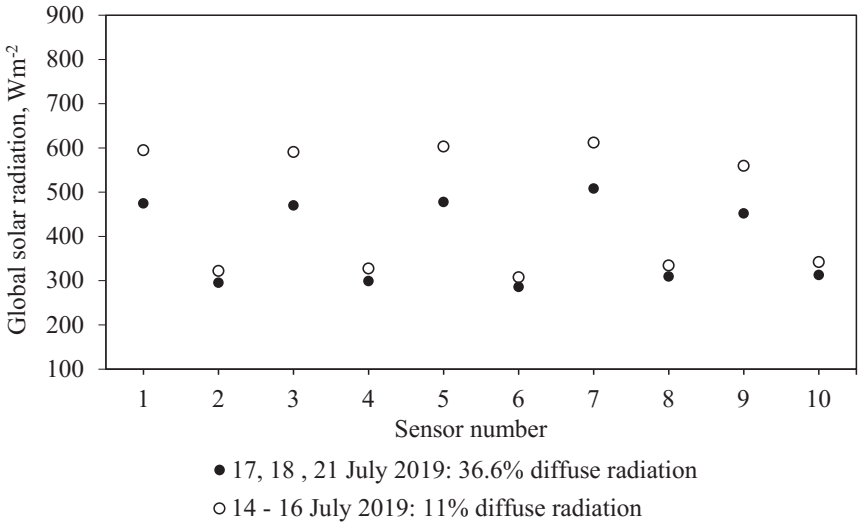

Fig. 4. Average values of global solar radiation along the centreline of the organic photovoltaic (OPV) tunnel in the middle of the growing season between 11:00 and 13:00 on sunny and cloudy days.

Table 2
Quantitative summary of the average radiation values at the meteorological station, in the control tunnel, and the organic photovoltaic (OPV) tunnel (average values of five shaded and five unshaded sensors) during sunny and cloudy days.

	Sunny days				Cloudy days			
	OPV tunnel		control tunnel	Meteorological station outside the tunnels	OPV tunnel		control tunnel	Meteorological station outside the tunnels
	Shaded sensors	Unshaded sensors			Shaded sensors	Unshaded sensors		
Average Values W m^{-2}	326.5	591.9	462.3	891.3	300.3	476.3	399.7	767.0
Std Dev W m^{-2}	25.9	41.2	28.1	22.7	40.3	66.2	52.1	103.8
Ratio In/Out	0.367	0.664	0.519		0.391	0.621	0.521	

Hence, on days with high diffuse radiation, light distribution within the OPV tunnel is more homogeneous, even though the light intensity is lower.

Table 2 summarises the data shown in Fig. 4, making it easy to see the average radiation values of the five shaded and five unshaded sensors during sunny and cloudy days. Additionally, the table provides data on the ambient radiation values that were measured by the meteorological station near the tunnels. The ratio between radiation inside and

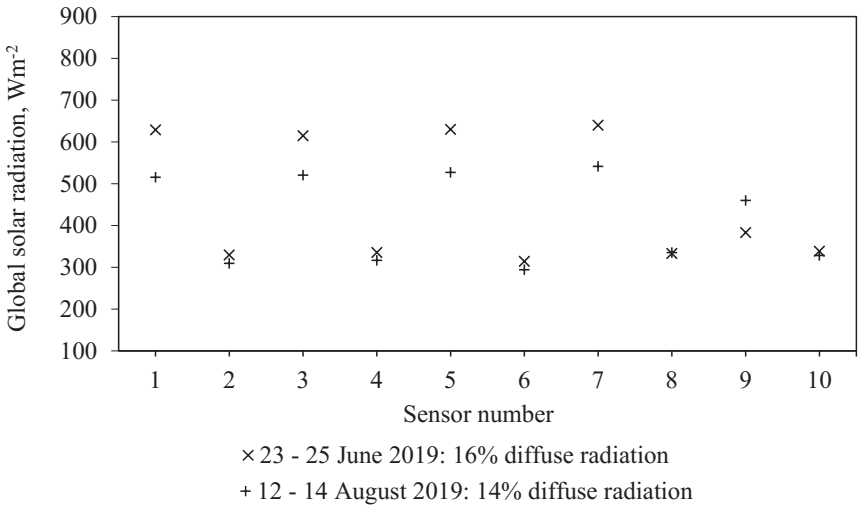

Fig. 5. Average values of global solar radiation along the centreline of the organic photovoltaic (OPV) tunnel between 11:00 and 13:00 on sunny days. × marks the beginning and +the end of the experimental period.

outside, as measured by the unshaded sensors, was higher on sunny days (ratio = 0.664) than on cloudy days with high diffusive radiation (ratio = 0.621). Conversely, the shaded sensors detected the opposite with a lower ratio on sunny days (ratio = 0.367) than on cloudy days (ratio = 0.391). The differences in the ratios between the shaded and unshaded sensors may be due to the different transmittance to diffuse radiation in polyethylene as compared with the OPV module material. Apparently, the transmittance of the OPV material to diffuse radiation is higher than that of the polyethylene sheet that covered the tunnel.

Fig. 5 examines the influence of the nonhomogeneous shading in the OPV tunnel on the radiation distribution in the tunnel centreline as a function of the solar elevation angle. Five sensors (sensor numbers: 2, 4, 6, 8, and 10) were shaded at the beginning of the experiment by the OPV modules, and the other five (sensor numbers: 1, 3, 5, 7, and 9) were placed between adjacent strips in the unshaded areas (see Fig. 1a). Differences in the average radiation values measured by the shaded and unshaded sensors at the beginning and end of the growing season are clear. Sensors that were unshaded at the beginning of the growing season became slightly shaded toward the end of the growing season (due to the change in the solar elevation angle during the season).

As expected in homogeneous shading by a shading net, the radiation along the centerline of the control tunnel was relatively uniform. The relations between values measured from sunrise to sunset, by two sensors placed 5 m apart, were $R_{G1} = 0.991R_{G2} - 3.2$ W m^{-2} ($R^2 = 0.996$) during three days at the beginning of the growing season 23–25 May 2019 and $R_{G1} = 1.01R_{G2} - 2.7$ W m^{-2} ($R^2 = 0.992$) during three days at the end of the growing season 20–22 August 2019.

The influence of the solar elevation angle on the shading of the sensors, is demonstrated in Fig. 6. The figure illustrates the effect of 5 OPV modules on the shading of 9 radiation sensors placed on the tunnel centreline 1.1 m beneath the tunnel ridge. Fig. 6a and b refer to the beginning and end of the growing season, respectively. At the beginning of the growing season, there was a distinct difference between the shaded and unshaded sensors at midday. Meanwhile, toward the end of the season, the unshaded sensors were closer to the shaded region at midday, and the difference between the shaded and unshaded sensors became small.

Fig. 7 examines the effect of the nonhomogeneous shading in the OPV tunnel as compared with the homogeneous shading in the control tunnel on the PAR values. On a specific day (21 August 2019), the PPFD values in the control tunnel were slightly higher than those in the OPV tunnel. Further, the radiation values at the time period around10:45 were slightly higher on the eastern side than on the western side and vice versa at the time period around 12:45. This was expected as the sun's position in the sky changes relative to the tunnel centreline. Note that the standard deviation values in the OPV tunnel were higher than those in the control owing to the less homogeneous light distribution along the paths between plant rows.

Fig. 8 compares the vertical and horizontal distributions of air temperature between both tunnels and examines the effect of ambient sunny (Fig. 8a) and cloudy (Fig. 8b) days on air temperature distributions. The figure shows the average air temperature values around noon (11:00–13:00) at different locations within the tunnels: 0.5 m and 2.4 m above the ground in the centre of the tunnel (centre bottom and centre top), and 1.3 m above the ground in the south, north, east, and west of each tunnel (Fig. 1). There was no significant difference in the average air temperature between the tunnels whether the days were sunny or

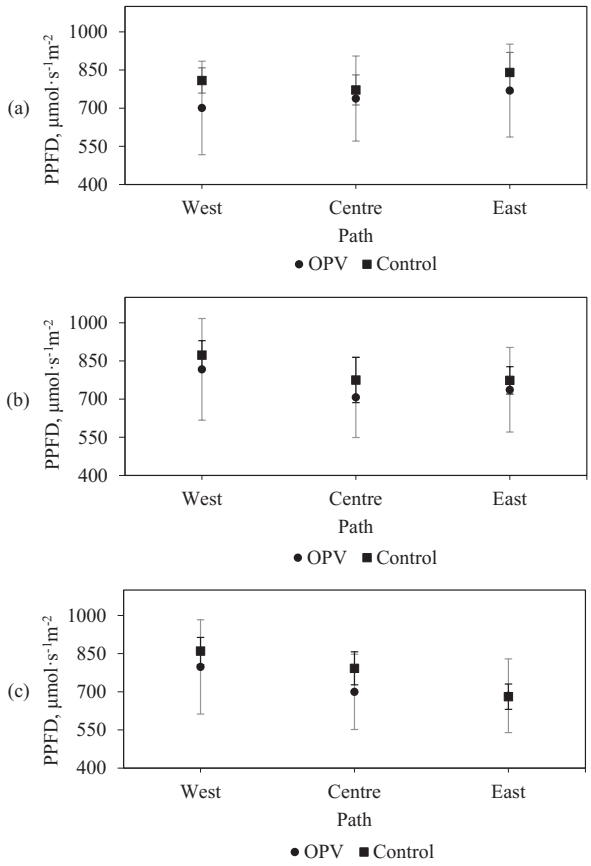

Fig. 7. Average values of photosynthetic photon flux density (PPFD) in the paths between adjacent plant rows in 21 August 2019 (a) measurements at 10:36–10:44 in the OPV tunnel and at 10:47–10:57 in the control tunnel, (b) measurements at 11:55–12:04 in the OPV tunnel and at 12:06–12:12 in the control tunnel, and (c) measurements at 12:48–12:57 in the OPV tunnel and at 12:59–13:06 in the control tunnel. Error bars represent standard deviation.

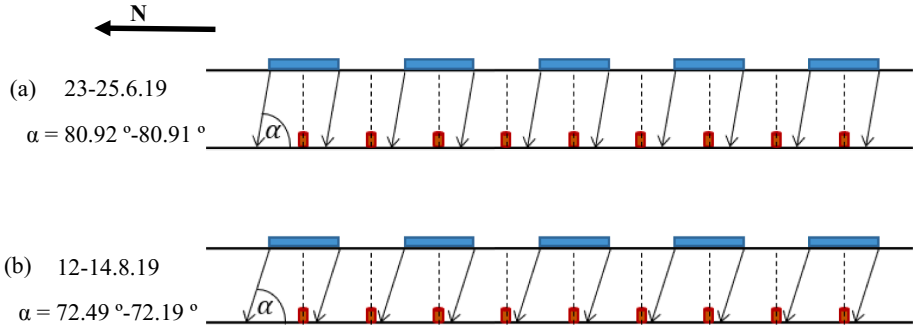

Fig. 6. Schematic view of the sensors transition from shaded/unshaded position to partial shading due to the change in solar elevation angle (α). June: 80.92–80.91°; August: 72.49–72.19°.

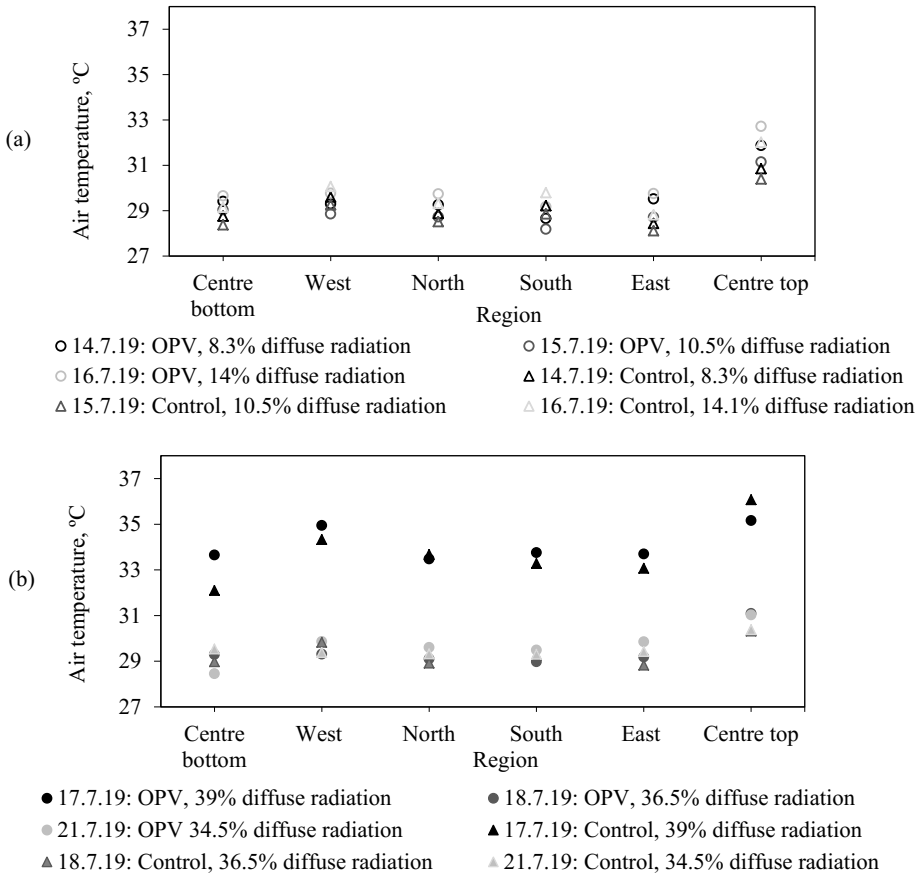

Fig. 8. Average air temperature measured by six sensors between 11:00 and 13:00 in both tunnels. Sensors were placed 0.5 m and 2.4 m above the ground in the centre of the tunnels (centre bottom and centre top, respectively). Four sensors were placed 1.3 m above the ground in the south, north, east, and west of each tunnel (see Fig. 1). (a) Sunny days and (b) cloudy days. Note that 17 July 2019 was an exceptionally hot day with an air temperature inside the tunnels higher than 32 °C.

cloudy. The temperature values at a height of 1.3 m were in the range of 29 ± 1 °C. On one extremely warm and cloudy day (17 July 2019), the temperatures within the tunnels were generally higher than 33 °C, revealing a similar pattern among the different measurement locations. Additionally, the temperature in the centre of the tunnel at the bottom was lower than the temperature at the top because of the temperature gradient caused by circulating warm air, which moves from the bottom to the top of the tunnel. Note that the temperature values measured in the plane 1.3 m above the ground (at different locations) were very similar.

Fig. 9 compares the vertical and horizontal distributions of VPD between both tunnels and examines the effect of ambient sunny (Fig. 9a) and cloudy (Fig. 9b) days in a manner similar to Fig. 8. Here, as well, there was no significant difference in the spatial variability of VPD between the OPV and control tunnels. Furthermore, the figure suggests that a change in the diffuse radiation did not significantly change the variability. In both tunnels, the VPD in the east was slightly lower than in the west. Approximately similar differences in VPD were observed in both tunnels between centre top and centre bottom.

Table 3 summarises the values of the different measured and calculated parameters used to determine the value of factor C (Equation (2)). This table provides data for four different days, revealing that C varied in the range of 0.90–0.99 in the control tunnel and 0.88–1.21 in the OPV tunnel. This suggests that there was a small difference in the closure of the energy balance between the tunnels. The largest difference in closure of the energy balance was observed on a cloudy day with a high percentage of diffuse radiation (42.1%). The deviations of the values of *C* in Table 3 from the value 1 were slightly smaller in the control tunnel than in the OPV tunnel. The root mean square deviation values from the value of 1 were 0.137 and 0.063 in the OPV and control tunnels, respectively. Sensible and latent heat fluxes were similar in the tunnels. The average values, of all four days, from Table 3 for the sensible heat flux in the control and OPV tunnels were 40.3 W m^{-2} and 36.7 W m^{-2}, respectively, while the average values of the latent heat flux were 276 W m^{-2} and 270 W m^{-2}, respectively. Hence, most of the net radiation was converted to latent heat, 76% and 84% in the control and OPV tunnels, respectively. Energy partitioning was virtually unaffected by the type of shading.

The following briefly summarizes the main agronomic results related to the crop performance under the OPV cover. More details are given in a previous paper by Friman-Peretz et al. (2020). The cumulative yield and average fruit weight in the OPV tunnel were very similar to those in the control greenhouse, which had a similar shading percentage. Furthermore, leaf area index, plant height and average canopy temperature were similar in the two tunnels. The leaf area index in the OPV tunnel varied between slightly smaller to slightly larger than in the control. OPV modules did not affect pollen viability as compared to pollen developed in the control tunnel. A slight non-significant improvement was observed in the total soluble solids (TSS) of fruits as compared to fruit developed in the control tunnel. Post-harvest quality assessment showed slightly better post-harvest parameters, with lower rotten fruits and a higher proportion of high-grade fruits in the OPV. On the other hand, under the OPV an inhibition of the red fruit color development was observed as compared to fruits from the control tunnel.

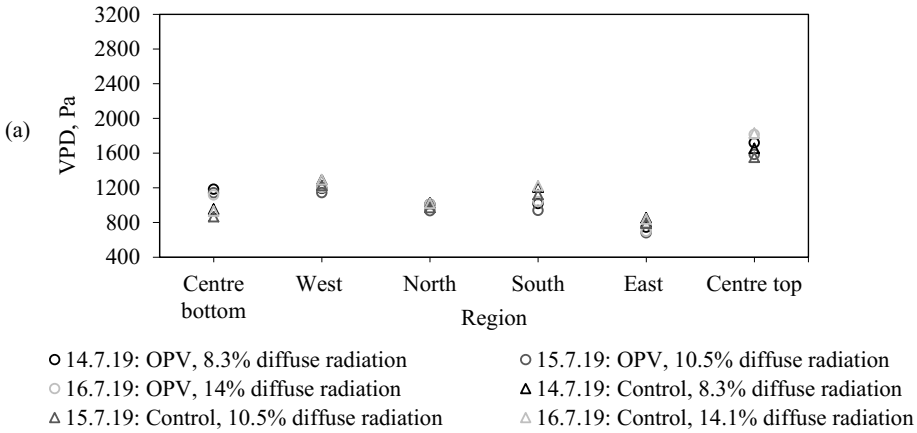

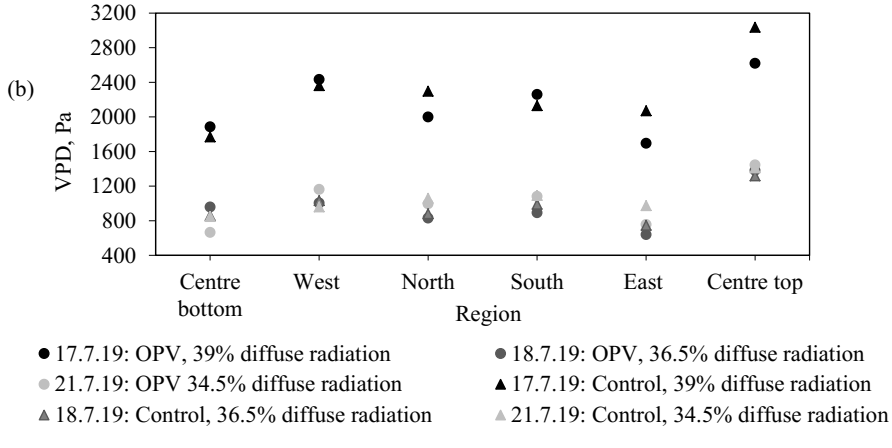

Fig. 9. Average VPD calculated by measurements from six sensors between 11:00 and 13:00 in both tunnels. Sensors were placed 0.5 m and 2.4 m above the ground in the centre of the tunnels (centre bottom and centre top, respectively). Four sensors were placed 1.3 m above the ground in the south, north, east, and west of each tunnel (see Fig. 1). (a) Sunny days and (b) cloudy days. Note that 17 July 2019 was an exceptionally hot day (See Fig. 8) with a VPD inside the tunnels higher than 1600 Pa.

Table 3
Values of the energy balance components in the organic photovoltaic (OPV) and control tunnels for 4 examined days (26 June, 3 July, 10 July and 7 August 2019). The average air temperature inside each tunnel was calculated from data obtained via four aspirated boxes in a horizontal plane (boxes 2, 3, 4, and 5; see Fig. 1). The values of all measured parameters in the table were calculated for times that correspond with the times at which T_{leaf} was measured in each tunnel.

Date	OPV				Control			
	26.6.19	3.7.19	10.7.19	7.8.19	26.6.19	3.7.19	10.7.19	7.8.19
R_{G0}, W m^{-2}	874.3	919.5	888.0	655.8	851.7	878.7	881.3	622.8
Diffuse radiation, %	8.9	8.2	14.7	42.1	8.9	8.2	14.7	42.1
T_0, ^oC	32.1	30.8	31.9	31.04	31.7	30.6	31.4	31.2
R.H.$_0$, %	54	52	55	56	55	54	57	56
U_0 m s^{-1}	1.1	1.7	1.5	1.5	1.1	1.5	1.7	1.3
T_a, ^oC	30.7	29.2	30.0	29.7	30.5	28.7	29.7	29.1
T_{leaf}, ^oC	32.5	29.6	31.7	30.1	32.5	30.3	31.5	29.9
R_G, W m^{-2}	441.3	462.5	446.2	278.4	479.5	480.4	471.0	285.3
LAI	3.66				3.02			
l, m	0.113				0.113			
VPD, kPa	1.37	1.15	1.11	1.37	1.33	1.16	1.12	1.18
r_a, s m^{-1}	66.2	63.3	69.4	66.1	85.1	93.3	96.7	81.9
r_c, s m^{-1}	92.6	91.2	95.4	144.3	72.3	73.7	77.8	102.7
Re	1269.7	1384.2	1154.1	1270.9	1125.8	936.6	873.2	1216.2
h, W ^{o} C^{-1} m^{-2}	17.6	18.4	16.8	17.6	13.7	12.5	12.0	14.2
R_n, W m^{-2}	360.3	367.5	347.2	211.4	410.3	400.1	372.0	261.6
G, W m^{-2}	24.8	18.0	28.1	32.1	21.8	26.6	28.8	26.2
λE, W m^{-2}	306.3	294.8	272.9	204.8	321.8	297.3	273.8	211.1
S, W m^{-2}	62.3	13.5	58.8	12.1	54.9	39.4	44.7	22.3
C	1.10	0.88	1.04	1.21	0.97	0.90	0.93	0.99

It is evident from present results and studies of other research groups that a possible solution to the problem of reduction in available PAR at canopy level, due to the cover of a greenhouse with conventional opaque PV panels, is the use of semitransparent PVs. The results of Friman-Peretz et al. (2020) suggested that under a Mediterranean climate, it is possible to grow tomatoes during summer in a greenhouse covered by semitransparent OPV modules, which cover about 40% of the roof area and result in about 25% irradiance reduction. A similar PV coverage ratio was reported by Ezzaeri et al. (2020) and Hassanien et al. (2018) for experiments with tomatoes. Like Friman-Peretz et al. (2020), these studies did not report any significant impact on the yield of the tomato plants.

Yet, the arrangement of the modules on the greenhouse cover is essential to obtain proper light distribution as suggested by Yano and Cossu (2019), Chen et al. (2019), Cossu et al. (2020), and references therein. Furthermore, the use of a greenhouse cover material with high light diffusion (as done in the present study) is recommended to allow better light penetration and distribution to lower layers of the canopy and is in agreement with the results of Tani et al. (2014). It appears that the present arrangement of the modules in strips, separated from each other by a distance equal to the strip width and using a polyethylene with high diffusion, contributed to a homogenous temperature and humidity distribution as well as a homogenous plant growth rate, similar to the observations in the control greenhouse. No significant effect on the air temperature and relative humidity, in comparison to a control greenhouse without PV panels, was also reported by Ezzaeri et al. (2020) and Ezzaeri et al. (2018) for 40% and 10% coverage of the roof area of a canary type greenhouse by PV panels respectively.

Further improvement of PV panels with respect to transparency in the PAR range and power conversion efficiency, could make their adoption to greenhouse cultivation more economically viable. In addition, it is recomanded to explore the percentage of shading suitable for each type of crop and adjust the PV shading accordingly, as suggested by Aroca-Delgado et al., (2018) and Poncet et al. (2012).

4. Conclusions

The effect of semitransparent flexible OPV modules placed on the top of a greenhouse tunnel on the spatial variability of radiation and air temperature and VPD was tested. The results show that strips of semitransparent OPV modules separated by a distance equal to their width, in conjunction with a diffuse polyethylene cover, successfully mitigated the a priori expected spatial variabilities in air temperature and VPD due to nonhomogeneous shading. However, the variability of radiation in the longitudinal direction of the OPV tunnel (parallel to the plant rows and perpendicular to the OPV strips) was high. Conversely, in the lateral direction, the variability in PAR radiation in the OPV tunnel was similar to that in the control. The spatial variability of radiation within the OPV tunnel, on days with a high percentage of diffuse solar radiation, was lower than on sunny days with low diffuse radiation. Moreover, the shading pattern from the OPV modules changed during the growing season as the solar elevation angle changed. At the beginning of the season, with a high solar elevation angle, variability in radiation along the OPV tunnel centreline was higher than toward the end of the season, when the elevation angle was smaller. Energy partitioning was virtually unaffected by the type of shading on sunny days with low diffuse radiation, and most of the net radiation, approximately 81 and 76% in the OPV and control respectively, were converted to latent heat. Additional experiments are needed to investigate whether the nonhomogeneous shading created by the OPV strips results in other significant physiological differences (e.g. transpiration and water consumption, photosynthesis) between plants in the shaded and unshaded areas. It is also of interest to determine the effect on the crop, of combining OPV modules with polyethylene covers with different haze properties. To reduce the nonhomogeneous shading on one hand and increase the electricity generation, on the other hand, it is advisable to aim for full coverage of the roof by semitransparent OPV modules. For that, production of OPV modules with high transmittance in the spectral ranges where photosynthesis efficiency is high is recommended.

Declaration of Competing Interest

The authors declare that they have no known competing financial interests or personal relationships that could have appeared to influence the work reported in this paper.

Acknowledgments

The authors thank the Chief Scientist of the Ministry of Agriculture and Rural Development of Israel (grant no. 20-12-0027, the BARD fund (grant no. US-4885-16), and the Plant Production and Marketing Board of Israel (grant no. 459-4540-17) for their support. Special thanks to Mrs Clara Shenderey for the help with data analysis and Dr. H. Yasour for help with measurements of agronomic aspects.

References

Aroca-Delgado, R., Perez-Alonso, J., Callejon-Ferre, A.J., 2018. Compatibility between crops and solar panels: an overview from shading systems. Sustainability 10, 743.
ASHRAE, Handbook of Fundamentals, 2005. American Society of heating, refrigerating and air-conditioning engineers. SI edition.
Baxevanou, C., Fidaros, D., Katsoulas, N., Mekeridis, E., Varlamis, C., Zachariadis, A., Logothetidis, S., 2020. Simulation of radiation and crop activity in a greenhouse covered with semitransparent organic photovoltaics. Applied Sciences 10 (7), 2550.
Chen, J., Xu, F., Ding, B., Wu, N., Shen, Z., Zhang, L., 2019. Performance analysis of radiation and electricity yield in a photovoltaic panel integrated greenhouse using the radiation and thermal models. Comput. Electron. Agric. 164, 104904.
Cossu, M., Ledda, L., Urracci, G., Sirigu, A., Cossu, A., Murgia, L., Pazzona, A., Yano, A., 2017a. An algorithm for the calculation of the light distribution in photovoltaic greenhouses. Sol. Energy 141, 38–48.
Cossu, M., Ledda, L., Deligios, P.A., Sirigu, A., Murgia, L., Pazzona, A., Yano, A., 2017b. Solar light distribution inside a greenhouse with the roof area entirely covered with photovoltaic panels. Acta Hortic. 1182, 47–56.
Cossu, M., Yano, A., Solinas, S., Deligios, P.A., Tiloca, M.T., Cossu, A., Ledda, L., 2020. Agricultural sustainability estimation of the European photovoltaic greenhouses. Eur. J. Agron. 118, 126074.
dos Reis Benatto, G.A., Corazza, M., Roth, B., Schütte, F., Rengenstein, M., Gevorgyan, S. A., Krebs, F.C., 2017. Inside or outside? linking outdoor and indoor lifetime tests of ITO-free organic photovoltaic devices for greenhouse applications. Energy Technol. 5 (2), 338–344.
Emmott, C.J., Röhr, J.A., Campoy-Quiles, M., Kirchartz, T., Urbina, A., Ekins-Daukes, N. J., Nelson, J., 2015. Organic photovoltaic greenhouses: a unique application for semitransparent PV? Energy Environ. Sci. 8 (4), 1317–1328.
Emmott, C.J., Moia, D., Sandwell, P., Ekins-Daukes, N., Hösel, M., Lukoschek, L., Amarasinghe, C., Krebs, F.C., Nelson, J., 2016. In-situ, long-term operational stability of organic photovoltaics for off-grid applications in Africa. Sol. Energy Mater. Sol. Cells 149, 284–293.
Ezzaeri, K., Fatnassi, H., Bouharroud, R., Gourdo, L., Bazgaou, A., Wifaya, A., Demrati, H., Bekkaoui, A., Aharoune, A., Poncet, C., Bouirden, L., 2018. The effect of photovoltaic panels on the microclimate and on the tomato production under photovoltaic canarian greenhouses. Sol. Energy 173, 1126–1134.
Ezzaeri, K., Fatnassi, H., Wifaya, A., Bazgaou, A., Aharoune, A., Poncet, C., Bekkaoui, A., Bouirden, L., 2020. Performance of photovoltaic canarian greenhouse: a comparison study between summer and winter seasons. Sol. Energy 198, 275–282.
Fatnassi, H., Poncet, C., Bazzano, M.M., Brun, R., Bertin, N., 2015. A numerical simulation of the photovoltaic greenhouse microclimate. Sol. Energy 120, 575–584.
Friman-Peretz, M., Geoola, F., Yehia, I., Ozer, S., Levi, A., Magadley, E., Brikman, R., Rosenfeld, L., Levy, A., Kacira, M., Teitel, M., 2019. Testing organic photovoltaic modules for application as greenhouse cover or shading element. Biosyst. Eng. 184, 24–36.
Friman-Peretz, M., Ozer, S., Geoola, F., Magadley, E., Yehia, I., Levi, A., Brikman, R., Gantz, S., Levy, A., Kacira, M., Teitel, M., 2020. Microclimate and crop performance in a tunnel greenhouse shaded by organic photovoltaic modules – comparison with conventional shaded and unshaded tunnels. Biosyst. Eng. 197, 12–31.
Hassanien, R.H.E., Li, M., Yin, F., 2018. The integration of semitransparent photovoltaics on greenhouse roof for energy and plant production. Renew. Energy 121, 377–388.
Magadley, E., Teitel, M., Friman-Peretz, M., Kacira, M., Yehia, I., 2020. Outdoor behaviour of organic photovoltaics on a greenhouse roof. Sustainable Energy Technol. Assess. 37, 100641.
Marucci, A., Monarca, D., Colantoni, A., Campiglia, E., Cappuccini, A., 2017. Analysis of the internal shading in a photovoltaic greenhouse tunnel. J. Agric. Eng. 48 (3), 154–160.
Monteith, J.L., Unsworth, M.H., 2013. Principles of Environmental Physics, fourth ed. Academic Press, New York.
Moretti, S., Marucci, A., 2019. A Photovoltaic Greenhouse with Variable Shading for the optimization of agricultural and energy production. Energies 12, 2589.

Murray, F.W., 1967. On the computation of saturation vapor pressure. J. Appl. Meteor. 6, 203–204.
Okada, K., Yehia, I., Teitel, M., Kacira, M., 2018. Crop production and energy generation in a greenhouse integrated with semitransparent organic photovoltaic film. Acta Hortic. 1227, 231–240.
Poncet, C., Muller, M.M., Brun, R., Fatnassi, H., 2012. Photovoltaic greenhouses, nonsense or a real opportunity for the greenhouse systems? Acta Hortic. 927, 75–79.
Tani, A., Shiina, S., Nakashima, K., Hayashi, M., 2014. Improvement in lettuce growth by light diffusion under solar panels. J. Agric. Meteorol. 70 (3), 139–149.
Teitel, M., 2017. Diurnal energy-partitioning and transpiration modelling in an insect-proof screenhouse with a tomato crop. Biosyst. Eng. 160, 170–178.
Tetens, O., 1930. Uber einige meteorologische Begriffe. Z Geophys. 6, 297–309.
Villarreal-Guerrero, F., Kacira, M., Fitz-Rodríguez, E., Kubota, C., Giacomelli, G.A., Linker, R., Arbel, A., 2012. Comparison of three evapotranspiration models for a greenhouse cooling strategy with natural ventilation and variable high pressure fogging. Sci. Hortic. 134, 210–221.
Yano, A., Cossu, M., 2019. Energy sustainable greenhouse crop cultivation using photovoltaic technologies. Renew. Sustain. Energy Rev. 109, 116–137.
Yang, F., Zhang, Y., Hao, Y., Cui, Y., Wang, W., Ji, T., Shi, F., Wei, B., 2015. Visibly transparent organic photovoltaic with improved transparency and absorption based on tandem photonic crystal for greenhouse application. Appl. Opt. 54 (34), 10232–10239.
Zhang, Y., Samuel, I.D.W., Wang, T., Lidzey, D.G., 2018. Current status of outdoor lifetime testing of organic photovoltaics. Adv. Sci. 5 (8), 1800434.